ISME

Cracked Piezoelectric Layer Bounded between Two Orthotropic Half-planes

M. Bastanfar[*]
Masters Student

M. Ayatollahi[†]
Professor

This paper deals with the behavior of anti-plane shear crack in a piezoelectric layer bounded between two orthotropic half-planes within the framework of linear electroelasticity. The crack surfaces are assumed to be permeable or impermeable. The analysis is based on the stress fields caused by electro-elastic dislocation in the medium. Fourier transforms are used to reduce the dislocation problem to the solution of Cauchy-type singular integral equations, which are solved numerically for the dislocation density on the cracks. The dislocation densities are then employed to derive field intensity factors at the crack tips. The results show that the stress and the electric displacement intensity factors at the crack tips depend on the lengths and orientation of the cracks. It is also shown that, for a fixed value of the mechanical load, the field intensity factor can be either enhanced depending on the magnitude and direction of the applied electrical load. Furthermore, the interaction between the two cracks is investigated.

Keywords: Anti-plane crack, Piezoelectric layer, Orthotropic half-planes, Field intensity factors, Singular integral equation

1 Introduction

Piezoelectric materials and structures have received significant attention due to the potential for designing adaptive structures that are both light in weight and possess adaptive control capabilities. Because of their brittleness, cracks in these materials are greatly concerned. Piezoelectric ceramics are bounded to composite components in many fields of modern technology. It is, thus, of great importance to study the fracture behavior of layered structures which are made of piezoelectric components. Cracked piezoelectric materials clearly consist multiple cracks with an extremely high crack density.
Therefore, the interaction between multiple cracks in piezoelectric materials plays an important role in the analysis and design of smart structures. An anti-plane shear crack in a piezoelectric layer bounded to dissimilar half-spaces under permeable crack-face conditions has been discussed using integral transform methods by Narita et al. [1].

[*] Masters Student, Faculty of Engineering, University of Zanjan, Zanjan, Iran , Marzieb1990@gmail.com
[†]Corresponding Author, Professor, Faculty of Engineering, University of Zanjan, Zanjan, Iran, mo.ayatollahy@gmail.com

Shin and Lee [2] considered the problem of a finite eccentric crack in a piezoelectric ceramic bounded two elastic half-planes. The investigation of two collinear anti-plane shear cracks in a piezoelectric layer bounded to half-planes has been studied by Zhou et al. [3]. In this paper the effect of the geometry of the two collinear cracks and piezoelectric constants upon the stress intensity factors have been studied. Kwon et al. [4] studied electromechanical behavior of an eccentric crack in a piezoelectric ceramic layer bounded between two elastic layers under anti-plane mechanical and in-plane electrical loadings. Ueda [5] considered the problem of a crack in a functionally graded piezoelectric material bounded to two elastic surface layers. Shenghu and Xing [6] treated the problem of a periodic array of parallel cracks in a homogeneous piezoelectric strip bounded to a FGP material.

Ding and Li [7] treated the problem of a periodic array of cracks in a functionally graded piezoelectric strip bounded to a homogeneous piezoelectric material. The effect of an imperfect interface on the fracture behavior of a layered piezoelectric was reported by Li and Lee [8]. They also concentrated mainly on the crack tip shielding and anti-shielding effects. The problem of a piezoelectric material containing a crack bounded to a FGPM material was considered by Ding et al. [9]. The plane deformation of a piezoelectric-piezomagnetic composite with two un-coaxial cracks parallel to the interface was examined by Li et al. [10]. The problem of cracked functionally graded piezoelectric layer was solved by Mousavi and Paavola [11]. These authors employed the distributed dislocation technique to solve the problem. Interaction between multiple cracks with arbitrary patterns in a piezoelectric strip reinforced with FGM coating under anti-plane loading was the subject of study by Bagheri et al. [12]. Recently Nourazar and Ayatollahi [13] obtained stress intensity factors for arbitrary oriented internal crack in an orthotropic layer bounded between two piezoelectric layers.

The main purpose of this study is to perform stress analysis of cracked piezoelectric layer which is bounded by two orthotropic layers. The distributed dislocation technique is utilized to perform a set of singular integral equations for the piezoelectric layer weakened by multiple cracks. These Cauchy singular integral equations are solved numerically by using Gauss-Chebyshev integration technique. The effects of geometry and material properties on field intensity factors are investigated.

2 Solution of electro-elastic dislocation

The dislocation problem under consideration is described in Fig.1. The piezoelectric layer is poled in the z-direction, which guarantees its transversely isotropic nature. Since the piezoelectric materials are polarized in the *z*-direction, the anti-plane elastic field is coupled with the in-plane electric field. The constitutive equations for piezoelectric materials in anti-plane problem can be written as:

$$\begin{aligned} &u(\mathrm{x},\mathrm{y})=0, \quad v(\mathrm{x},\mathrm{y})=0, \quad w=w(x,y), \\ &E_x=E_x(x,y), \quad E_y=E_y(x,y), \quad E_z=0. \end{aligned} \tag{1}$$

For a piezoelectric material, the following coupled electromechanical equations hold

$$\begin{Bmatrix} \sigma_{zx}(x,y) \\ \sigma_{zy}(x,y) \end{Bmatrix} = c_{44} \begin{Bmatrix} \dfrac{\partial w}{\partial x} \\ \dfrac{\partial w}{\partial y} \end{Bmatrix} + e_{15} \begin{Bmatrix} \dfrac{\partial \varphi}{\partial x} \\ \dfrac{\partial \varphi}{\partial y} \end{Bmatrix},$$

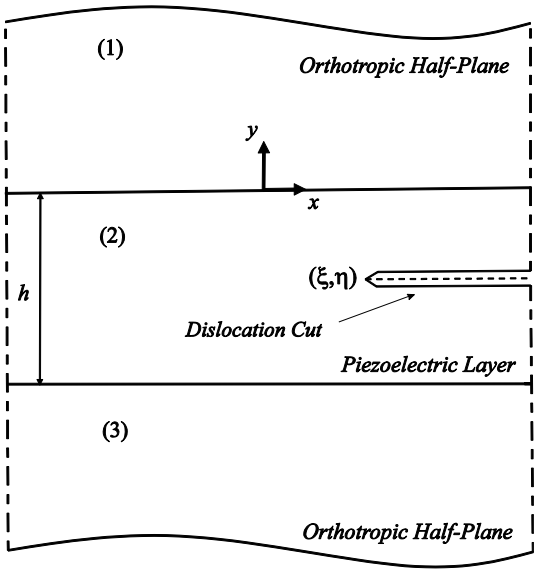

Figure 1 A schematic of a medium containing electromechanical dislocations.

$$\begin{Bmatrix} D_x(x,y) \\ D_y(x,y) \end{Bmatrix} = e_{15} \begin{Bmatrix} \dfrac{\partial w}{\partial x} \\ \dfrac{\partial w}{\partial y} \end{Bmatrix} - d_{11} \begin{Bmatrix} \dfrac{\partial \varphi}{\partial x} \\ \dfrac{\partial \varphi}{\partial y} \end{Bmatrix}. \tag{2}$$

where D_i, $(i = x, y)$ and φ represent the components of electric displacements, and electric potential, respectively, c_{44}, e_{15} and d_{11} are the shear modulus, piezoelectric coefficient and dielectric parameter.

The piezoelectricity problem requires the solution of the following equilibrium equations:

$$\begin{aligned} &c_{44}\nabla^2 w(x,y) + e_{15}\nabla^2 \varphi(x,y) = 0, \\ &e_{15}\nabla^2 w(x,y) - d_{11}\nabla^2 \varphi(x,y) = 0, \qquad -h < y < 0. \end{aligned} \tag{3}$$

In the above equations, ∇^2 is the two dimensional Laplacian operator. It should be note that body forces and free charge are neglected in this study. Suppose that the cracks are electrically impermeable. Then, the boundary and continuity conditions for the elastic and electric field are taken to be:

$$\begin{aligned} \lim_{|y|\to\infty} \sigma_{zx}(x,y) = \lim_{|y|\to\infty} \sigma_{zy}(x,y) = \lim_{|y|\to\infty} w(x,y) = 0, \\ D_y(x,0^-) = 0, D_y(x,-h^+) = 0, \\ \sigma_{yz}(x,-h^+) = \sigma_{yz}(x,-h^-), \\ w_2(x,-h^+) = w_3(x,-h^-), \\ \sigma_{yz}(x,0^+) = \sigma_{yz}(x,0^-), \\ w_1(x,0^+) = w_2(x,0^-), \qquad |x| < \infty. \end{aligned} \tag{4}$$

The conditions representing the screw and electric dislocations are expressed by:

$$\sigma_{yz}(x,\eta^+)=\sigma_{yz}(x,\eta^-),$$
$$D_y(x,\eta^+)=D_y(x,\eta^-). \tag{5a}$$
$$w_2(x,\eta^+)-w_2(x,\eta^-)=b_z H(x-\xi),$$
$$\varphi_2(x,\eta^+)-\varphi_2(x,\eta^-)=b_\varphi H(x-\xi), \qquad |x|<\infty. \tag{5b}$$

In which $H(.)$ being the Heaviside-step function, superscripts + and – denote upper and lower edges of the cut, respectively. The Eqs. (5a), enforce the continuity of tractions and electric displacement while the Eqs. (5b) implies the multi valuedness of displacement and electric potential. In the case of permeable conditions, the electric potential is continuous in the lower and upper edges of the cut. To obtain the stress and electric displacement fields induced by the continuously distributed dislocation, one needs to solve the problem of single dislocation. By using the standard Fourier transforms, the solution of Eq. (3) may be obtained as:

$$w(x,y)=\frac{1}{2\pi}\int_{-\infty}^{\infty}[A_1(s)\cosh(sy)+A_2(s)\sinh(sy)]e^{isx}ds, \qquad \eta<y\le 0,$$
$$\varphi(x,y)=\frac{1}{2\pi}\int_{-\infty}^{\infty}[A_3(s)\cosh(sy)+A_4(s)\sinh(sy)]e^{isx}ds, \qquad \eta\le y<0,$$
$$w(x,y)=\frac{1}{2\pi}\int_{-\infty}^{\infty}[B_1(s)\cosh(sy)+B_2(s)\sinh(sy)]e^{isx}ds, \qquad -h<y\le\eta,$$
$$\varphi(x,y)=\frac{1}{2\pi}\int_{-\infty}^{\infty}[B_3(s)\cosh(sy)+B_4(s)\sinh(sy)]e^{isx}ds, \qquad -h\le y<\eta. \tag{6}$$

Where the coefficients $A_i(s),B_i(s),i=1,2,3,4$ are unknown. These unknown functions will be determined from the boundary conditions (4) and (5). Thus, after obtaining the displacement components and electric potential expressions, the stresses and the electric displacements are as follows:

$$\sigma_{zy}(x,y)=\frac{b_\varphi e_{15}}{\pi}\int_0^\infty \sin[s(x-\xi)]\frac{\sinh[s(h+\eta)]\sinh(sy)}{\sinh(sh)}ds$$
$$+\frac{b_z}{2\pi}\int_0^\infty \sin[s(x-\xi)]\frac{2\sinh(sh)L_1[\alpha c_{44}\sinh(sy)-(\beta c_{44}+\gamma e_{15})\cosh(sy)]-\gamma e_{15}\sinh(sy)R_1}{\sinh(sh)K_1}ds,$$
$$\sigma_{zx}(x,y)=\frac{b_\varphi e_{15}}{\pi}\int_0^\infty \cos[s(x-\xi)]\frac{\sinh[s(h+\eta)]\cosh(sy)}{\sinh(sh)}ds$$
$$+\frac{b_z}{2\pi}\int_0^\infty \cos[s(x-\xi)]\frac{2\sinh(sh)L_1[\alpha c_{44}\cosh(sy)-(\beta c_{44}+\gamma e_{15})\sinh(sy)]-\gamma e_{15}\cosh(sy)R_1}{\sinh(sh)K_1}ds,$$
$$D_x(x,y)=-\frac{b_\varphi d_{11}}{\pi}\int_0^\infty \cos[s(x-\xi)]\frac{\cosh(sy)\sinh[s(h+\eta)]}{\sinh(sh)}ds$$
$$+\frac{b_z}{2\pi}\int_0^\infty \cos[s(x-\xi)]\frac{\gamma d_{11}\cosh(sy)R_1+2e_{15}\alpha\sinh(sh)\cosh(sy)L_1}{\sinh(sh)K_1}ds,$$
$$D_y(x,y)=-\frac{b_\varphi d_{11}}{\pi}\int_0^\infty \sin[s(x-\xi)]\frac{\sinh(sy)\sinh[s(h+\eta)]}{\sinh(sh)}ds$$

$$+\frac{b_z}{2\pi}\int_0^{\infty}\sin[s(x-\xi)]\frac{\gamma d_{11}\sinh(\mathrm{sy})R_1+2e_{15}\alpha\sinh(\mathrm{sy})\sinh(sh)L_1}{\sinh(sh)K_1}ds,\qquad \eta<y<0. \tag{7a}$$

and

$$\sigma_{zy}(\mathrm{x},\mathrm{y})=\frac{b_z}{\pi}\int_0^{\infty}\sin[\mathrm{s}(\mathrm{x}-\xi)]\{\frac{\mathrm{c}_{44}[\alpha\cosh(sh)+\beta\sinh(sh)]\sinh(\mathrm{sy})F_1}{K_1}$$
$$-\frac{\gamma e_{15}(\alpha\sinh[s(h+\eta)]+\beta\cosh[s(h+\eta)])\cosh(\mathrm{sy})}{K_1}$$
$$+\frac{2\mathrm{c}_{44}\sinh(sh)[\alpha\sinh(sh)+\beta\cosh(sh)]\cosh(\mathrm{sy})F_1-\gamma e_{15}\sinh(\mathrm{sy})R_1}{2\sinh(sh)K_1}\}\mathrm{ds}$$
$$+\frac{b_\varphi e_{15}}{\pi}\int_0^{\infty}\sin[\mathrm{s}(\mathrm{x}-\xi)]\frac{\sinh(s\eta)\sinh[\mathrm{s}(\mathrm{y}+h)]}{\sinh(sh)}\mathrm{ds},$$

$$\sigma_{zx}(\mathrm{x},\mathrm{y})=\frac{b_z}{\pi}\int_0^{\infty}\cos[\mathrm{s}(\mathrm{x}-\xi)]\{\frac{\mathrm{c}_{44}[\alpha\sinh(sh)+\beta\cosh(sh)]\sinh(\mathrm{sy})F_1}{K_1}$$
$$-\frac{\gamma e_{15}(\alpha\sinh[s(h+\eta)]+\beta\cosh[s(h+\eta)])\sinh(\mathrm{sy})}{K_1}$$
$$+\frac{2\mathrm{c}_{44}[\alpha\cosh(sh)+\beta\sinh(sh)]\sinh(sh)\cosh(\mathrm{sy})F_1-\gamma e_{15}\cosh(\mathrm{sy})R_1}{2\sinh(sh)K_1}\}ds$$
$$+\frac{b_\varphi e_{15}}{\pi}\int_0^{\infty}\cos[\mathrm{s}(\mathrm{x}-\xi)]\frac{\sinh(s\eta)\cosh[s(h+y)]}{\sinh(sh)}\mathrm{ds},$$

$$D_x(\mathrm{x},\mathrm{y})=\frac{b_z}{\pi}\int_0^{\infty}\cos[\mathrm{s}(\mathrm{x}-\xi)]\{\frac{e_{15}(\alpha\cosh(sh)+\beta\sinh(sh))\cosh(\mathrm{sy})F_1}{K_1}$$
$$+\frac{2e_{15}[\alpha\sinh(sh)+\beta\cosh(sh)]\sinh(sh)\sinh(\mathrm{sy})F_1+\gamma d_{11}\cosh(\mathrm{sy})R_1}{2\sinh(sh)K_1}$$
$$+\frac{\gamma d_{11}(\alpha\sinh[s(h+\eta)]+\beta\cosh[s(h+\eta)])\sinh(\mathrm{sy})}{K_1}\}ds$$
$$-\frac{b_\varphi d_{11}}{\pi}\int_0^{\infty}\cos[\mathrm{s}(\mathrm{x}-\xi)]\frac{\sinh(s\eta)\cosh[s(h+y)]}{\sinh(sh)}ds,$$

$$D_y(\mathrm{x},\mathrm{y})=\frac{b_z}{\pi}\int_0^{\infty}\sin[s(x-\xi)]\{\frac{e_{15}(\alpha\cosh(sh)+\beta\sinh(sh))\sinh(\mathrm{sy})F_1}{K_1}$$
$$+\frac{2e_{15}[\alpha\sinh(sh)+\beta\cosh(sh)]\sinh(sh)\cosh(\mathrm{sy})F_1+\gamma d_{11}\sinh(\mathrm{sy})R_1}{2\sinh(sh)K_1}$$
$$+\frac{\gamma d_{11}(\alpha\sinh[s(h+\eta)]+\beta\cosh[s(h+\eta)])\cosh(\mathrm{sy})}{K_1}\}ds$$
$$-\frac{b_\varphi d_{11}}{\pi}\int_0^{\infty}\sin[s(x-\xi)]\frac{\sinh(s\eta)\sinh[\mathrm{s}(h+\mathrm{y})]}{\sinh(sh)}ds,\qquad -h<y<\eta. \tag{7b}$$

where

$$
\begin{aligned}
L_1 &= \alpha \sinh[s(h+\eta)] + \beta \cosh[s(h+\eta)],\\
R_1 &= \alpha[3\sinh(s\eta) + \sinh[s(2h+\eta)]] - \beta[\cosh(s\eta) - \cosh[s(2h+\eta)]],\\
F_1 &= \alpha \sinh(s\eta) - \beta \cosh(s\eta),\\
K_1 &= \sinh(sh)(\alpha^2 + \beta^2) + 2\alpha\beta \cosh(sh).
\end{aligned}
\tag{7c}
$$

and $\alpha = \mathrm{d}_{11}\,\mathrm{c}_{44} + \mathrm{e}_{15}^2$, $\beta = G_y\, g\, \mathrm{d}_{11}$, $\gamma = g\, G_y\, e_{15}$. Also $g^2 = G_x/G_y$ is the ratio of material properties of the half-planes. By observing that the equations 7(a) and 7(b) have the form:

$$
F(x,y) = \int_0^\infty G(y,s) \begin{Bmatrix} \sin[\mathrm{s}(x-\xi)] \\ \cos[\mathrm{s}(x-\xi)] \end{Bmatrix} ds \tag{8}
$$

If we let $G_\infty(y,s)$ be the leading term in the asymptotic form of $G(y,s)$ for $s \to \infty$, $F(x,y)$ can be expressed as:

$$
F(x,y) = F_s(x,y) + F_b(x,y) \tag{9}
$$

It is expected that the kernels will exhibit certain singular behavior. Thus, a detailed asymptotic analysis of the nature of singularities is needed. The integrals giving the kernels in Eq.(8) show divergent behavior for $s \to \infty$. These divergent parts of the kernels may be separated by inquiring the asymptotic behavior of the integrands.

$$
F_s(x,y) = \int_{-\infty}^\infty G_\infty(y,s) \begin{Bmatrix} \cos[\mathrm{s}(x-\xi)] \\ \sin[\mathrm{s}(x-\xi)] \end{Bmatrix} ds \tag{10}
$$

$$
F_b(x,y) = \int_{-\infty}^\infty [G(y,s) - G_\infty(y,s)] \begin{Bmatrix} \cos[\mathrm{s}(x-\xi)] \\ \sin[\mathrm{s}(x-\xi)] \end{Bmatrix} ds \tag{11}
$$

Where $\mathrm{F_s}$ is the singular part of the kernel and $\mathrm{F_b}$ is the bounded functions. The singular behavior of the field components is determined by the asymptotic values of the integrands in Eqs. (7a) and (7b) for $s \to \infty$. The details of the analysis will not be given in this paper. The leading terms of asymptotic expansions of the integrands in Eqs. (7a) and (7b) are the following appropriate forms [14]:

$$
\begin{aligned}
\sigma_{zy\infty}(x,\mathrm{y}) &= -\frac{b_z\,\mathrm{c}_{44} + b_\varphi e_{15}}{2\pi} \frac{x-\xi}{(x-\xi)^2 + (y-\eta)^2},\\
\sigma_{zx\infty}(\mathrm{x},\mathrm{y}) &= \frac{b_z\,\mathrm{c}_{44} + b_\varphi e_{15}}{2\pi} \frac{y-\eta}{(x-\xi)^2 + (y-\eta)^2},\\
D_{x\infty}(\mathrm{x},\mathrm{y}) &= \frac{b_z\, e_{15} - b_\varphi d_{11}}{2\pi} \frac{y-\eta}{(x-\xi)^2 + (y-\eta)^2},\\
D_{y\infty}(x,y) &= \frac{b_\varphi d_{11} - b_z\, e_{15}}{2\pi} \frac{x-\xi}{(x-\xi)^2 + (y-\eta)^2}, \qquad \eta < y < 0,\\
\sigma_{zy\infty}(x,y) &= -\frac{b_z\,\mathrm{c}_{44} + b_\varphi e_{15}}{2\pi} \frac{x-\xi}{(x-\xi)^2 + (y-\eta)^2},\\
\sigma_{zx\infty}(\mathrm{x},\mathrm{y}) &= \frac{b_z\, c_{44} + b_\varphi e_{15}}{2\pi} \frac{y-\eta}{(x-\xi)^2 + (y-\eta)^2},\\
D_{x\infty}(\mathrm{x},\mathrm{y}) &= \frac{b_z\, e_{15} - b_\varphi d_{11}}{2\pi} \frac{y-\eta}{(x-\xi)^2 + (y-\eta)^2},
\end{aligned}
$$

$$D_{y\infty}(\mathrm{x},\mathrm{y})=\frac{b_\varphi d_{11}-b_z e_{15}}{2\pi}\frac{x-\xi}{(x-\xi)^2+(y-\eta)^2},\qquad -h<y<\eta. \tag{12}$$

It may be considered that the stress and electric displacement components have the standard Cauchy type singularities at the dislocation location. By adding and subtracting the asymptotic expressions of integrands, the stress and electric displacement components are found as follows:

$$\sigma_{zy}(\mathrm{x},\mathrm{y})=-\frac{c_{44}b_z+e_{15}b_\varphi}{2\pi}\{\frac{x-\xi}{(x-\xi)^2+(y-\eta)^2}$$
$$+\int_0^\infty \sin[s(x-\xi)]e^{s(\eta-y)}(\frac{(1-e^{2ys})(1-e^{-2s(h+\eta)})}{1-e^{-2hs}}-1)ds\},$$
$$\sigma_{zx}(\mathrm{x},\mathrm{y})=\frac{c_{44}b_z+e_{15}b_\varphi}{2\pi}\{\frac{y-\eta}{(x-\xi)^2+(y-\eta)^2}$$
$$+\int_0^\infty \cos[s(x-\xi)]e^{s(\eta-y)}[\frac{(1+e^{2ys})(1-e^{-2s(h+\eta)})}{1-e^{-2hs}}-1]ds\},$$
$$D_x(\mathrm{x},\mathrm{y})=\frac{e_{15}b_z-d_{11}b_\varphi}{2\pi}\{\frac{y-\eta}{(x-\xi)^2+(\mathrm{y}-\eta)^2}$$
$$+\int_0^\infty \cos[s(x-\xi)]e^{s(\eta-y)}[\frac{(1+e^{2ys})(1-e^{-2s(h+\eta)})}{1-e^{-2hs}}-1]ds\},$$
$$D_y(\mathrm{x},\mathrm{y})=-\frac{e_{15}b_z-d_{11}b_\varphi}{2\pi}\{\frac{x-\xi}{(x-\xi)^2+(\mathrm{y}-\eta)^2}$$
$$+\int_0^\infty \sin[s(x-\xi)]e^{s(\eta-y)}[\frac{(1-e^{2ys})(1-e^{-2s(h+\eta)})}{1-e^{-2hs}}-1]ds\},\quad \eta<y<0,$$
$$\sigma_{zy}(x,y)=-\frac{c_{44}b_z+e_{15}b_\varphi}{2\pi}\{\frac{(x-\xi)}{(y-\eta)^2+(x-\xi)^2}$$
$$+\int_0^\infty \sin[\mathrm{s}(\mathrm{x}-\xi)]\mathrm{e}^{s(y-\eta)}[\frac{(1-\mathrm{e}^{-2s(h+y)})(1-\mathrm{e}^{2s\eta})}{1-e^{-2hs}}-1]ds\},$$
$$\sigma_{zx}(x,y)=-\frac{b_z c_{44}+b_\varphi e_{15}}{2\pi}\{-\frac{y-\eta}{(y-\eta)^2+(x-\xi)^2}$$
$$+\int_0^\infty \cos[\mathrm{s}(\mathrm{x}-\xi)]\mathrm{e}^{s(y-\eta)}[\frac{(e^{-2s(h+y)}+1)(1-\mathrm{e}^{2s\eta})}{1-e^{-2hs}}-1]ds\},$$
$$D_x(x,y)=-\frac{e_{15}b_z-d_{11}b_\varphi}{2\pi}\{-\frac{y-\eta}{(\mathrm{x}-\xi)^2+(y-\eta)^2}$$
$$+\int_0^\infty \cos[\mathrm{s}(\mathrm{x}-\xi)]\mathrm{e}^{s(y-\eta)}[\frac{(1+e^{-2s(h+y)})(1-\mathrm{e}^{2s\eta})}{1-e^{-2hs}}-1]ds\},$$
$$D_y(x,y)=-\frac{e_{15}b_z-d_{11}b_\varphi}{2\pi}\{\frac{\mathrm{x}-\xi}{(\mathrm{x}-\xi)^2+(y-\eta)^2}$$
$$+\int_0^\infty \sin[\mathrm{s}(\mathrm{x}-\xi)]\mathrm{e}^{s(y-\eta)}[\frac{(1-\mathrm{e}^{-2s(h+y)})(1-\mathrm{e}^{2s\eta})}{1-e^{-2hs}}-1]ds\},\quad -h<y<\eta.$$

(13)

For computational efficiency it may also be more convenient to evaluate the kernels in appropriate exponential forms. It is seen that for $s \to \infty$ all integrals in Eq. (13) decay quickly, which makes the integrals susceptible to numerical evaluation. For permeable case, it is sufficient to let the jump in the electric potential be zero.

3 The singular integral equations

Let N be the number of cracks in the medium. The curved cracks configurations with respect to the Cartesian coordinate may be expressed in parametric form as:

$$\begin{aligned} x_i &= x_i(s), \\ y_i &= y_i(s), \quad i \in \{1,2,...,N\} \quad -1 \le s \le 1 \end{aligned} \tag{14}$$

Two movable orthogonal coordinate systems s-*n* are chosen on the i-th crack such that their origin locate on the cracks while the *s*-axis remains tangent to the cracks surface. The stress and electric components should be transformed to the s-n coordinate on the i-the crack. Assume screw dislocations with unknown density are distributed on the infinitesimal segment $\sqrt{[x_j'(t)]^2 + [y_j'(t)]^2}\,dt$ of the surface of j-th crack. The following integral equations are obtained:

$$\begin{aligned} \sigma_{zn}(x_i(s), y_i(s)) &= \sum_{j=1}^{N} \int_{-1}^{1} [K_{ij}^{11}(s,t) B_{zj}(t) + K_{ij}^{12}(s,t) B_{pj}(t)] \sqrt{[x_j'(t)]^2 + [y_j'(t)]^2}\,dt, \\ D_n(x_i(s), y_i(s)) &= \sum_{j=1}^{N} \int_{-1}^{1} [K_{ij}^{21}(s,t) B_{zj}(t) + K_{ij}^{22}(s,t) B_{pj}(t)] \sqrt{[x_j'(t)]^2 + [y_j'(t)]^2}\,dt, \quad n = \{x, y\} \end{aligned} \tag{15}$$

where $B_{zj}(t)$ and B_{pj} are the dislocation densities on the non-dimensionalized length $-1 \le t \le 1$. and the known kernels are given in the Appendix. The left hand side of the Eqs. (15) are stress and electric displacement components at the supposed location of the cracks with negative sign. The integral equations must be solved under the following single-valuedness conditions:

$$\begin{aligned} w_j^-(s) - w_j^+(s) &= \int_{-1}^{s} \sqrt{[x_j'(t)]^2 + [y_j'(t)]^2}\, B_{zj}(t)\,dt, \\ \varphi_j^-(s) - \varphi_j^+(s) &= \int_{-1}^{s} \sqrt{[x_j'(t)]^2 + [y_j'(t)]^2}\, B_{pj}(t)\,dt. \end{aligned} \tag{16}$$

The displacement field is single-valued out of surfaces of embedded cracks. So, Cauchy singular integral Eqs. (15) should be complemented by closure requirements

$$\int_{-1}^{1} \sqrt{[x_j'(t)]^2 + [y_j'(t)]^2}\, B_{kj}(t)\,dt = 0, \qquad k \in \{z, p\} \tag{17}$$

The singular integral equations (15) are solved numerically by using (17) and an appropriate collocation technique to determine dislocation density functions. From (15), it is seen that the dominant part of the integral has a simple Cauchy kernel and consequently, the solution may be expressed as:

$$B_{kj}(t) = \frac{g_{kj}(t)}{\sqrt{1-t^2}}, \quad -1 \le t \le 1, \quad k \in \{z, p\} \tag{18}$$

where $g_{kj}(t)$ is bounded and $g_{kj}(\pm 1) \neq 0,\ (k = z, p)$. The function $g_{kj}(t)$ are obtained via solution of the system of equations. The field intensity factors for the i-th embedded crack are [12]:

$$\begin{Bmatrix} (K_M)_{Li} \\ (K_M)_{Ri} \end{Bmatrix} = \pm \frac{L_i(\mp)}{2}[c_{44} g_{zi}(\mp 1) + e_{15} g_{pi}(\mp 1)]$$
$$\begin{Bmatrix} (K_D)_{Li} \\ (K_D)_{Ri} \end{Bmatrix} = \pm \frac{L_i(\mp)}{2}[e_{15} g_{zi}(\mp 1) - d_{11} g_{pi}(\mp 1)] \tag{19}$$

where $L_i(\mp) = [[x_i'(\mp 1)]^2 + [y_i'(\mp 1)]^2]^{\frac{1}{4}}$ The details of the derivation of field intensity factors to reach (19) are not given here.

4 Results and discussions

The main interest in this study is in evaluating the effect of loading conditions, cracks interaction and geometric size on field intensity factor in the piezoelectric layer bounded to orthotropic half-planes. The field intensity factors are normalized with $K_{0D} = (\tau_0 e_{15}/c_{44})\sqrt{L}$ and $K_0 = \tau_0\sqrt{L}$. Where L is the half length of crack. In Table (1), the material properties of piezoelectric layer is presented.

The eletromechanical coupling factor is defined by $\lambda = \frac{D_0 e_{15}}{\tau_0 d_{11}}$. In the proceeding example, unless otherwise stated, the medium is assumed to be loaded by constant loading $\sigma_{yz} = \tau_0,\ D_y = D_0$ which are distributed on the boundaries. In this section we first present some results calculated to verify the analytical solution. The validity of results is illustrated by solving four examples.

The problem of an anti-plane shear crack in a piezoelectric layer bonded to dissimilar half-planes solved by Narita et al. [1] is re-examined and the results are displayed in Fig. (2).
As it may be seen, the agreement of the results in the above example is excellent. The next verification of analysis is established by considering a crack with length 2L which is parallel to the piezoelectric layer boundary under permeable condition.
As it may be observed in Fig. 3, the results of these analyses are in quite good agreement with the results given by Shin and Lee [2].

Table 1 The material properties

	PZT-4	*PZT-5*	*PZT-5H*	*Epoxy*
$c_{44}(\frac{N}{m^2})$	2.56×10^{10}	2.11×10^{10}	2.3×10^{10}	0.176
$e_{15}(\frac{C}{m^2})$	12.7	12.3	17.0	0
$d_{11}(\frac{C}{Vm})$	64.6×10^{-10}	8.11×10^{-9}	150.4×10^{-10}	–

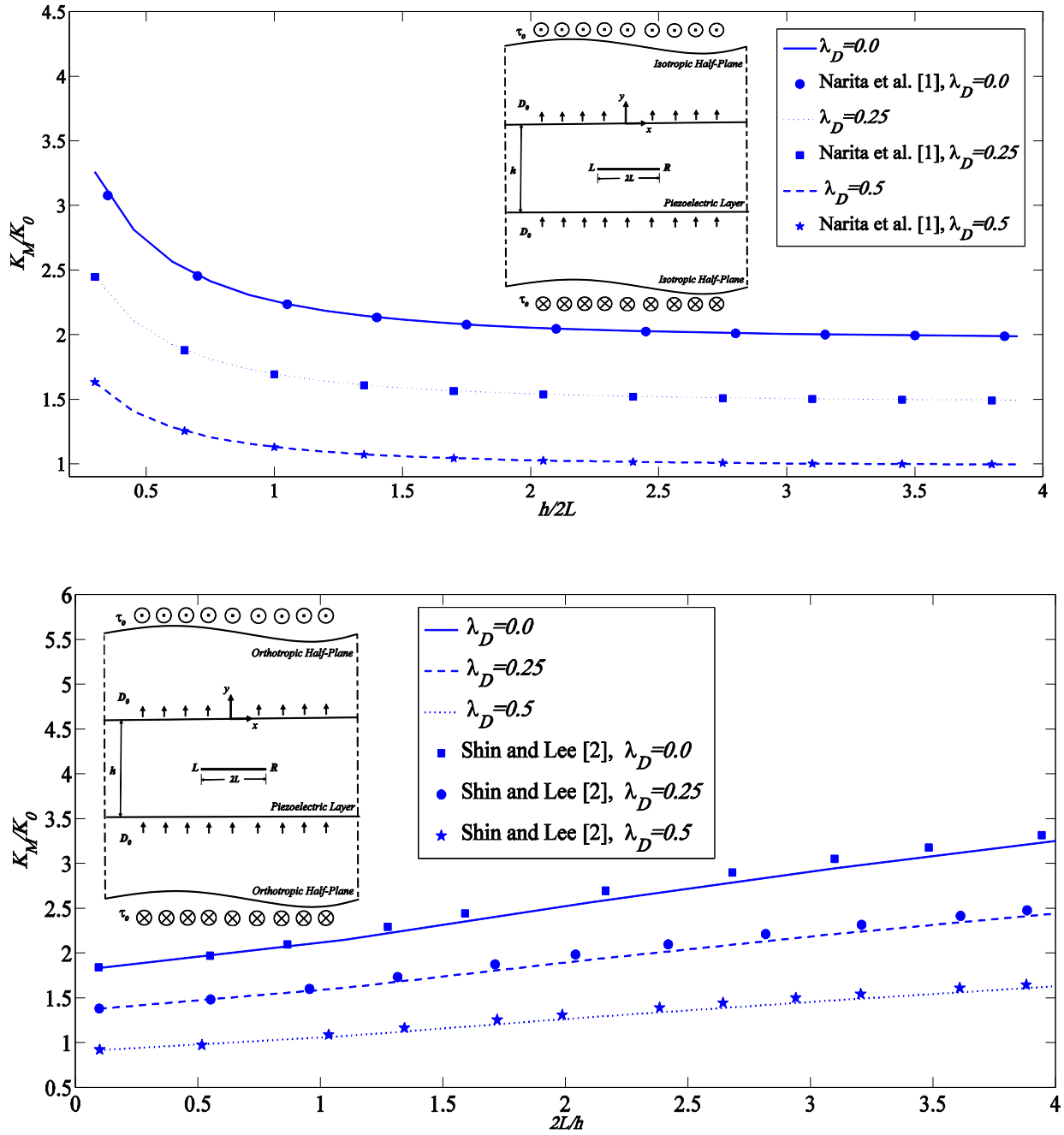

Figure 3 Dimensionless stress intensity factors versus $2L/h$.

The values of normalized stress intensity factor for eccentric crack in a piezoelectric strip bounded to half-planes are presented in Fig. (4). The results closely match those obtained for the same problem by Shin and Lee [2].

The last verification is performed by considering two equal-length collinear cracks with length 2L which are situated on the center-line of the piezoelectric layer Fig. (5). The results are compared with the solution of a cracked piezoelectric layer bounded to two elastic half-planes obtained by Zhou et al. [3]. As it may be observed, except for small value of b, the results of these analyses have in reasonable agreement.

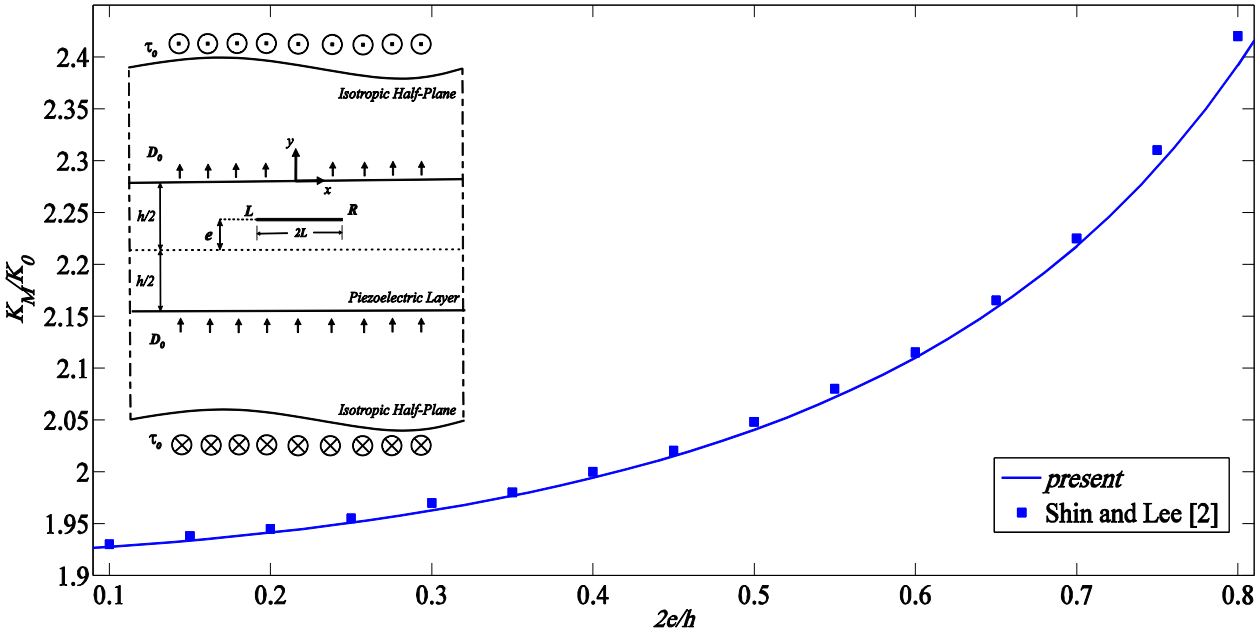

Figure 4 Dimensionless stress intensity factors versus $2e/h$.

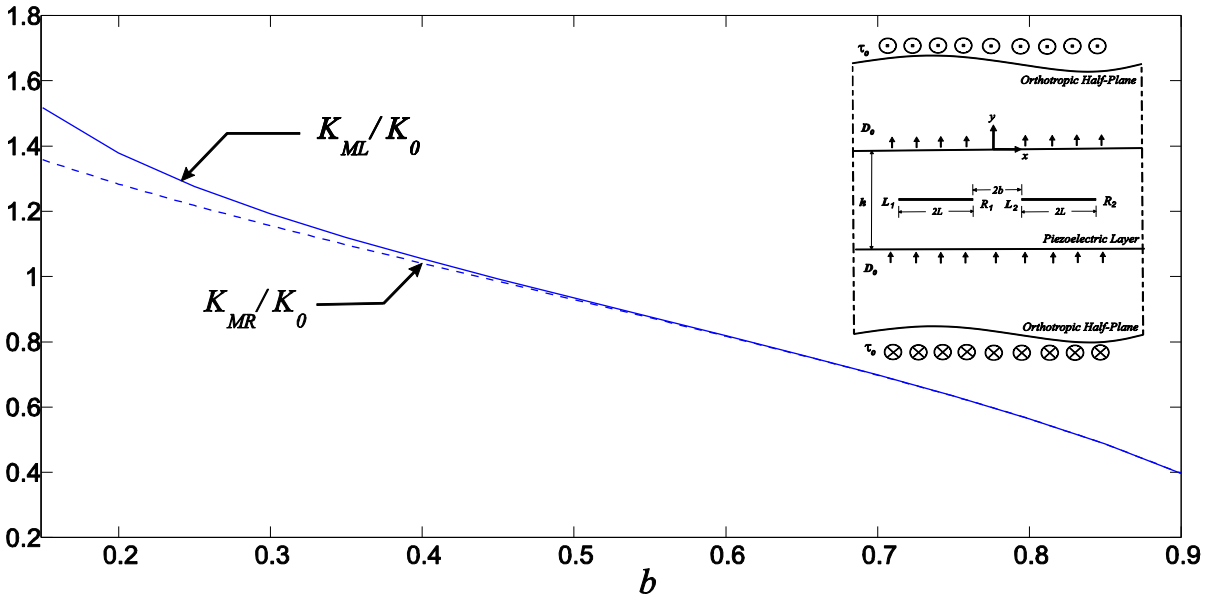

Figure 5 Dimensionless stress intensity factors for two collinear cracks

Fig. (6). illustrates the effect of crack orientation on the normalized field intensity factors. The electromechanical coupling factor was assumed to be $\lambda = 0.5$. The crack located on the center-line of the piezoelectric layer. It is seen that, as θ increase the normalized field intensity factor first decrease obviously from relatively high values and then at $\theta = \pi/2$ tend to zero.

At $\theta = \pi/2$, the loading is parallel to the crack, consequently, the traction on the crack surface vanishes. Therefore, the field intensity factors are zero. The center line of the piezoelectric layer is the line of symmetry and the field intensity factors for crack tips are identical.

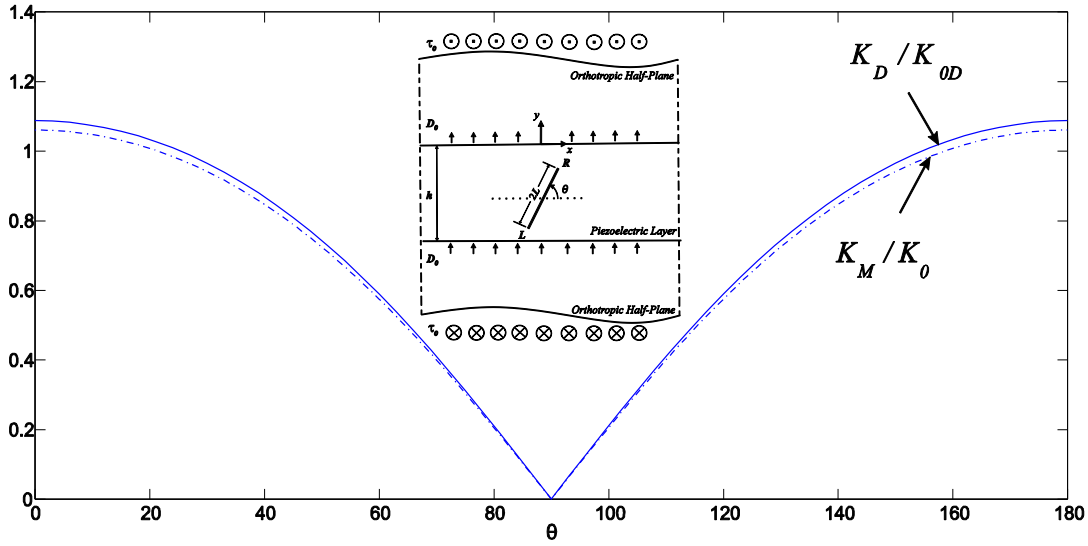

Figure 6 Dimensionless field intensity factors for an oblique crack.

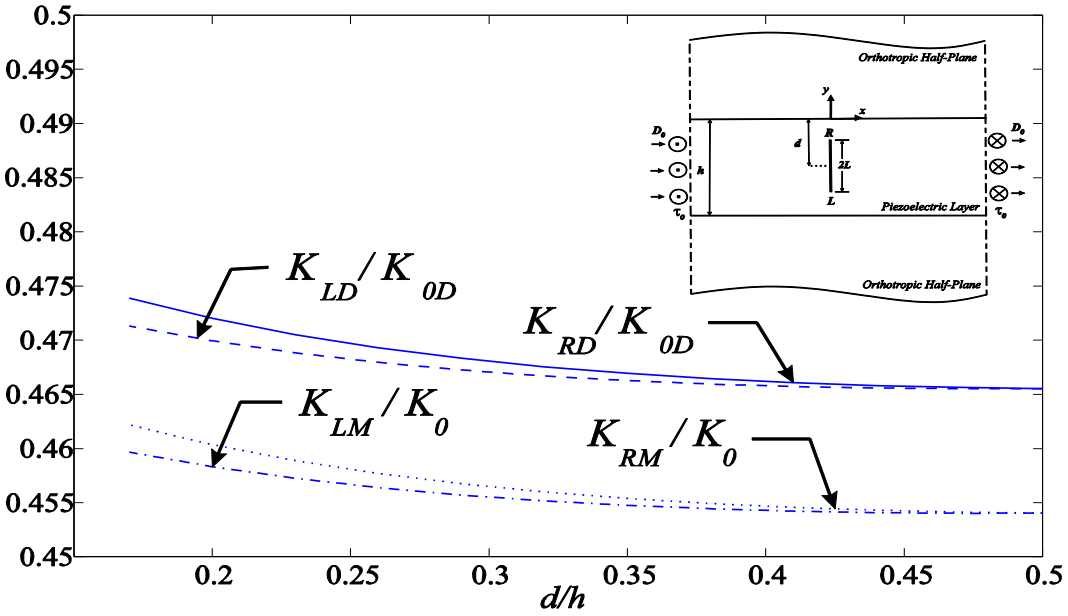

Figure 7 Dimensionless field intensity factors for a vertical crack.

The field intensity factors for a crack perpendicular to the piezoelectric boundary are plotted in Fig. (7). for different values of d/h. The results were calculated for a constant value of the crack length 2L=0.01m. The same observations can be made when varying the parameter *h* instead of the parameter d. It can be found that, the dimensionless field intensity factors decrease with the increase in d/h.

The different between the results of K_L and K_R decrease rapidly as the d/h approaches to the 0.5. This phenomenon is caused by the symmetry of the problem.

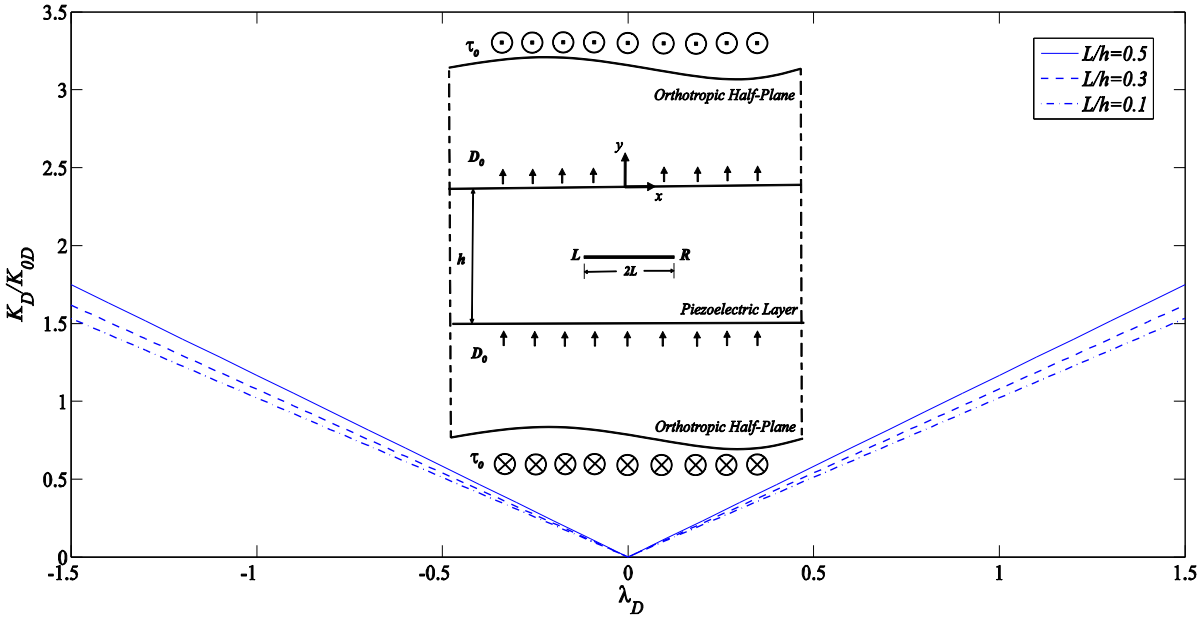

Figure 8 Dimensionless electric intensity factors versus electromechanical coupling factor.

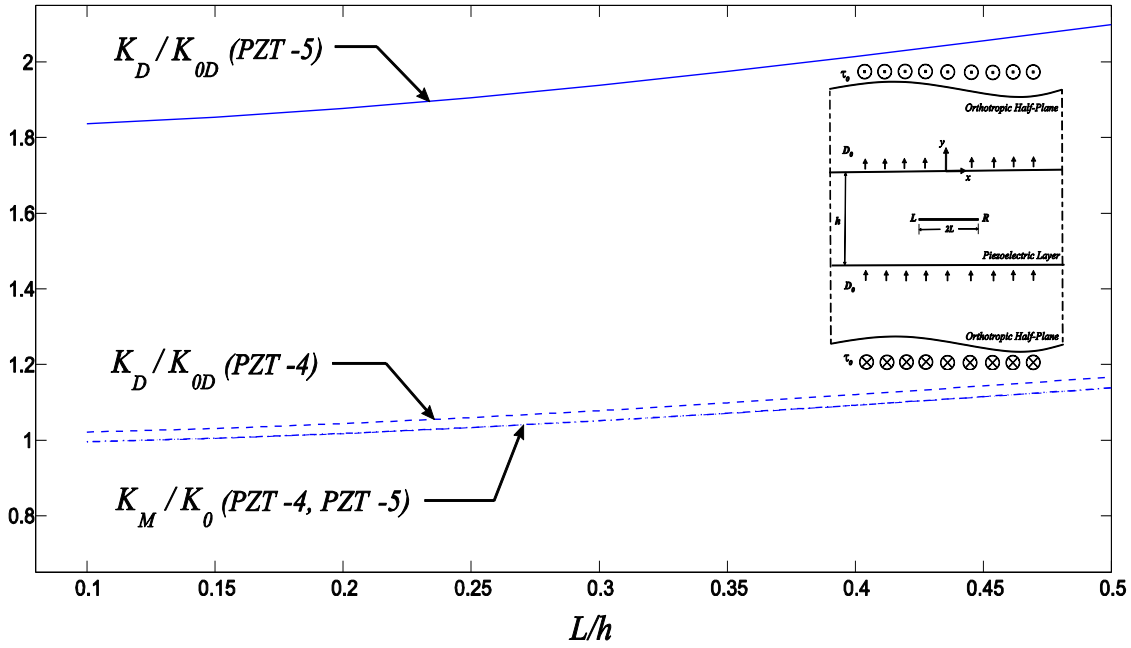

Figure 9 Dimensionless field intensity factor for a parallel crack versus crack length.

Fig. (8). depicts the normalized electric intensity factor versus electromechanical coupling factor. It follows from the obtained results that decreasing the value of the electromechanical coupling factor results in a decrease in the electric intensity factor.

Fig. (9). displays the variation of the normalized field intensity factors against the normalized crack length for various piezoelectric material. The effect of material properties on stress intensity factor is negligible, but is noticeable on electric intensity factor.

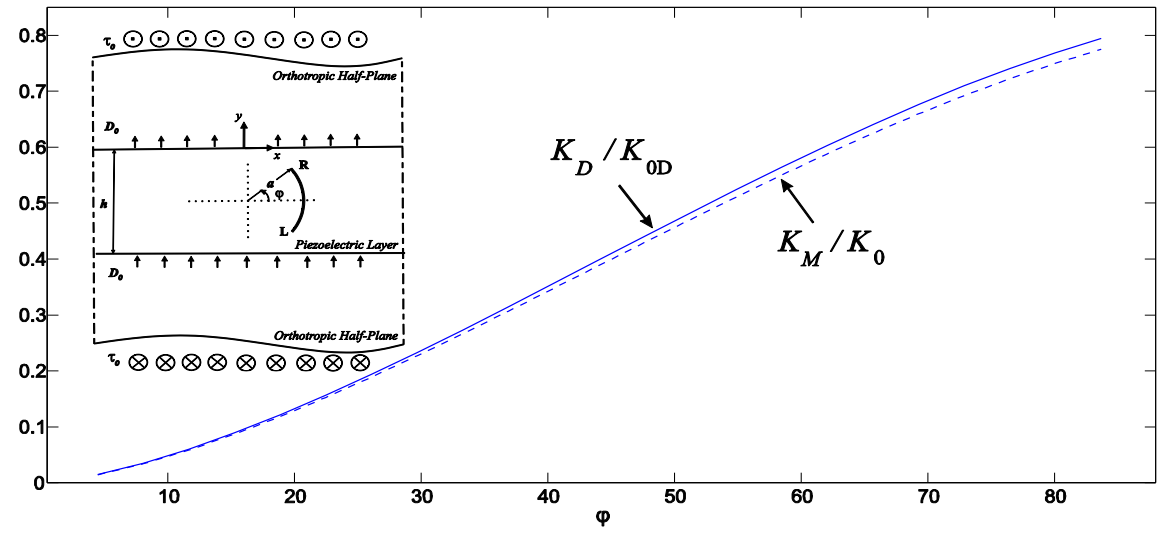

Figure 10 Dimensionless field intensity factor for a curved crack.

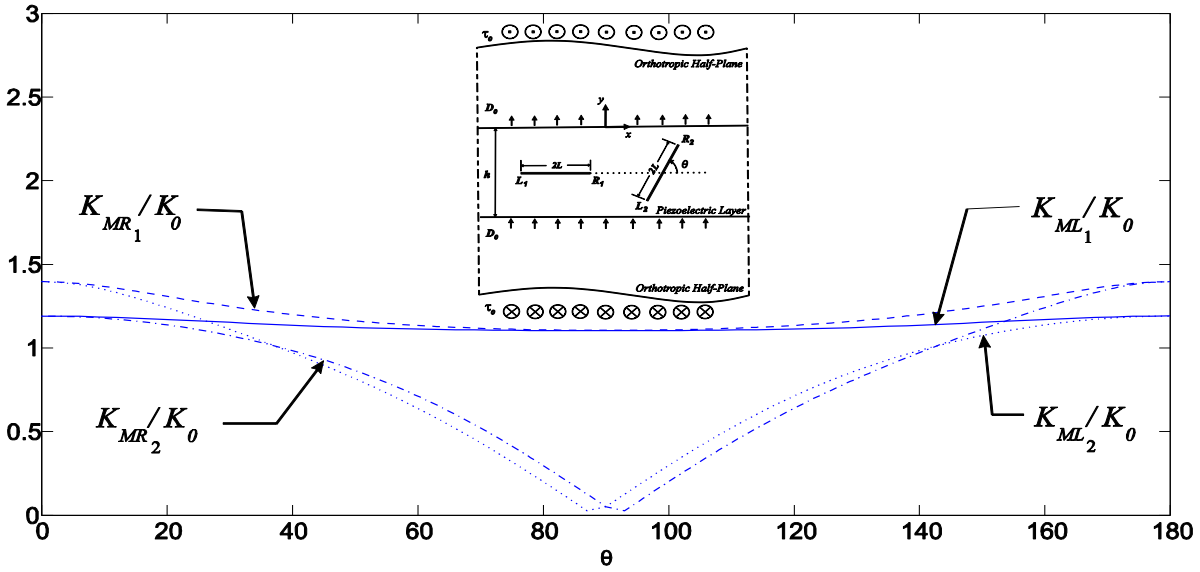

Figure 11 Dimensionless stress intensity factor for an oblique crack and parallel crack.

In the following example a curved crack which are portions of the circumference of a circle is considered. The variation of normalized field intensity factors against φ is depicted in Fig. (10). It may be seen that increasing the value of φ while keeping a and h constant tends to increase the field intensity factor. It is evident from this figure that decreasing the value of φ, which means that the crack length become short, leads to a reduction of the field intensity factors which become zero corresponding to the case of zero crack length. The variation of field intensity factors manifest the same trend.

Fig. (11). exhibits the variation of stress intensity factor with the interaction of two cracks. The cracks L_1R_1 is fixed whereas crack L_2R_2 is changing orientation. As expected, stress intensity factors are functions of second crack orientations.

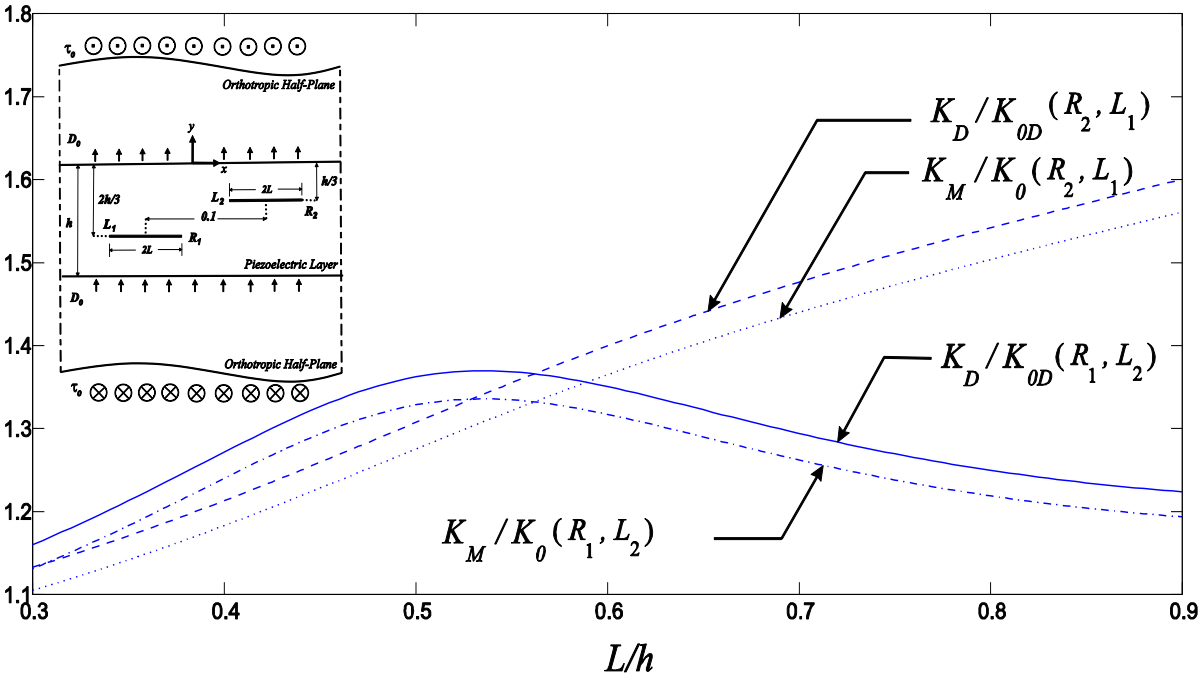

Figure 12 Dimensionless field intensity factors for parallel off-center cracks.

For $\theta = \pi/2$, the traction vanishes on L_2R_2 but the interaction between cracks produces small values of stress intensity factor of crack tips.

Two off-center equal-length cracks which are parallel to the piezoelectric layer boundary are depicted in Fig. (12). In this case, the results were obtained for a constant value of the cracks center distance 0.1 m while the cracks lengths are changing with the same rate. It is observed that, the maximum field intensity factor for the crack tips R_1 and L_2 occur when the distance between them is minimum.

5 Concluding remarks

The fracture behavior of a piezoelectric layer bounded between two orthotropic containing multiple cracks is investigated using the method of distributed dislocation technique. The distributed dislocation technique is used to derive singular integral equations for analyzing a cracked piezoelectric layer. Two types of electric boundary conditions on the crack surface are considered. The computational results show that the type of piezoelectric layer has significant effect on the electric displacement intensity factor, but it has little effect on the stress intensity factor. The field intensity factors always increase with the increase of crack length. Also the field intensity factors depend on the magnitudes and directions of electrical loads.

References

[1] Narita, F., Shindo, Y., and Watanabe, K., "Anti-plane Shear Crack in a Piezoelectric Layer Bonded to Dissimilar Half-spaces", JSME International Journal Series A Solid Mechanics and Material Engineering, Vol. 42, pp. 66-72, (1999).

[2] Shin, J.W., and Lee, K.Y., "Eccentric Crack in a Piezoelectric Strip Bonded to Half-planes", European Journal of Mechanics A/solids, Vol. 19, pp. 989-994, (2000).

[3] Zhou, Z.G., Chen, J.Y., and Wang, B., "Analysis of Two Collinear Cracks in a Piezoelectric Layer Bonded to Two Half Spaces Subjected to Anti-plane Shear", Meccanica, Vol. 35, pp. 443-456, (2000).

[4] Kwon, S.M., Son, M.S., and Lee, K.Y., "Transient Behavior in a Cracked Piezoelectric Layered Composite: Anti-plane Problem", Mechanics of Materials, Vol. 34, pp. 593-603, (2002).

[5] Ueda, S., "Crack in Functionally Graded Piezoelectric Strip Bonded to Elastic Surface Layers under Electro Mechanical Loading", Theoretical and Applied Fracture Mechanics, Vol. 40, pp. 225-236, (2003).

[6] Shenghu, D., and Xing, L., "The Periodic Crack Problem in Bonded Piezoelectric Materials", Acta Mechanica Solida Sinica, Vol. 20, pp. 171-179, (2007) .

[7] Ding, S.H., and Li, X., "Periodic Cracks in a Functionally Graded Piezoelectric Layer Bonded to a Piezoelectric Half-plane", Theoretical and Applied Fracture Mechanics, Vol. 49, pp. 313-320, (2008).

[8] Li, Y.D., and Lee, K.Y., "Crack Tip Shielding and Anti-shielding Effects of the Imperfect Interface in a Layered Piezoelectric Sensor", International Journal of Solids and Structures, Vol. 46, pp. 1736-1742, (2009).

[9] Ding, S.H., Li, X., and Guo, L.F., "Analysis of Bonded Piezoelectric Materials with a Crack Perpendicular to the Interface Subjected to In-plane Loading", Computational Material Science, Vol. 47, pp. 977-984, (2010).

[10] Li, Y.D., Zhao, H., and Zhang, N., "Mixed Mode Fracture of a Piezoelectric–piezomagnetic Bi-layer Structure with Two Un-coaxial Cracks Parallel to the Interface and each in a Layer", International Journal of Solids and Structures, Vol. 50, pp. 3610-3617, (2013).

[11] Mousavi, S.M., and Paavola, J., "Analysis of Cracked Functionally Graded Piezoelectric Strip", International Journal of Solids and Structures, Vol. 50, pp. 2449–2456, (2013).

[12] Bagheri, R., Ayatollahi, M., and Mousavi, S.M., "Analysis of Cracked Piezoelectric Layer with Imperfect Non-homogeneous Orthotropic Coating", International Journal of Mechanical Sciences, Vol. 93, pp. 93-101, (2015).

[13] Nourazar, M., and Ayatollahi, M., "Analysis of an Orthotropic Strip Containing Multiple Defects Bonded between Two Piezoelectric Layers", Acta Mechanica, Vol. 227, pp. 1293-1306, (2016).

[14] Abramowitz, M., and Stegun, I.A., "*Handbook of Mathematical Functions*", Dover, New York, (1972).

Nomenclature

b_z, b_φ	Burgers vector
B_{zj}, B_{pj}	Dislocation densities
E_x, E_y, E_z	The electric fields
$g_{zj}(t), g_{pj}(t)$	Regular terms of dislocation densities
h	Thickness of piezoelectric layer
$H(.)$	Heaviside step function
K_{ij}^{lm}	Kernels of integral equations
K_M, K_D	Field intensity factor of crack tips
N	Total number of cracks
u, v, w	The displacement fields
$x_i(s), y_i(s)$	Functions describing the geometry of cracks
φ	Electric Potential
σ_{zx}, σ_{zy}	The anti-plane stress components

Appendix

The coefficients in Eq. (15)

$$K_{ij}^{11} = -\frac{c_{44}}{2\pi}\{\frac{x_i - x_j}{(x_i - x_j)^2 + (y_i - y_j)^2} + \int_0^\infty \sin[s(x_i - x_j)]e^{-s(y_i - y_j)}[\frac{(1-e^{2sy_i})(1-e^{-2s(h+y_j)})}{1-e^{-2hs}} - 1]ds\}\cos\theta_i$$

$$-\frac{c_{44}}{2\pi}\{\frac{y_i - y_j}{(x_i - x_j)^2 + (y_i - y_j)^2} + \int_0^\infty \cos[s(x_i - x_j)]e^{-s(y_i - y_j)}[\frac{(1+e^{2sy_i})(1-e^{-2s(h+y_j)})}{1-e^{-2hs}} - 1]ds\}\sin\theta_i,$$

$$K_{ij}^{12} = -\frac{e_{15}}{2\pi}\{\frac{x_i - x_j}{(x_i - x_j)^2 + (y_i - y_j)^2} + \int_0^\infty \sin[s(x_i - x_j)]e^{-s(y_i - y_j)}[\frac{(1-e^{2sy_i})(1-e^{-2s(h+y_j)})}{1-e^{-2hs}} - 1]ds\}\cos\theta_i$$

$$-\frac{e_{15}}{2\pi}\{\frac{y_i - y_j}{(x_i - x_j)^2 + (y_i - y_j)^2} + \int_0^\infty \cos[s(x_i - x_j)]e^{-s(y_i - y_j)}[\frac{(1+e^{2sy_i})(1-e^{-2s(h+y_j)})}{1-e^{-2hs}} - 1]ds\}\sin\theta_i,$$

$$K_{ij}^{21}=-\frac{e_{15}}{2\pi}\{\frac{x_i-x_j}{(x_i-x_j)^2+(y_i-y_j)^2}$$

$$+\int_0^\infty \sin[s(x_i-x_j)]e^{-s(y_i-y_j)}[\frac{(1-e^{2sy_i})(1-e^{-2s\left(h+y_j\right)})}{1-e^{-2hs}}-1]ds\}\cos\theta_i$$

$$-\frac{e_{15}}{2\pi}\{\frac{y_i-y_j}{(x_i-x_j)^2+(y_i-y_j)^2}$$

$$+\int_0^\infty \cos[s(x_i-x_j)]e^{-s(y_i-y_j)}[\frac{(1+e^{2sy_i})(1-e^{-2s\left(h+y_j\right)})}{1-e^{-2hs}}-1]ds\}\sin\theta_i,$$

$$K_{ij}^{22}=\frac{d_{11}}{2\pi}\{\frac{x_i-x_j}{(x_i-x_j)^2+(y_i-y_j)^2}$$

$$+\int_0^\infty \sin[s(x_i-x_j)]e^{-s(y_i-y_j)}[\frac{(1-e^{2sy_i})(1-e^{-2s(h+y_j)})}{1-e^{-2hs}}-1]ds\}\cos\theta_i$$

$$+\frac{d_{11}}{2\pi}\{\frac{y_i-y_j}{(x_i-x_j)^2+(y_i-y_j)^2}$$

$$+\int_0^\infty \cos[s(x_i-x_j)]e^{-s(y_i-y_j)}[\frac{(1+e^{2sy_i})(1-e^{-2s(h+y_j)})}{1-e^{-2hs}}-1]ds\}\sin\theta_i,\qquad y_j<y_i<0,$$

$$K_{ij}^{11}=-\frac{c_{44}}{2\pi}\{\frac{(x-x_j)}{(y-y_j)^2+(x-x_j)^2}$$

$$+\int_0^\infty \sin[s(x_i-x_j)]e^{s(y-y_j)}[\frac{(1-e^{-2s(h+y_i)})(1-e^{2sy_j})}{1-e^{-2hs}}-1]ds\}\cos\theta_i$$

$$+\frac{c_{44}}{2\pi}\{-\frac{y-y_j}{(y-y_j)^2+(x-x_j)^2}$$

$$+\int_0^\infty \cos[s(x_i-x_j)]e^{s(y-y_j)}[\frac{(1+e^{-2s(h+y_i)})(1-e^{2sy_j})}{1-e^{-2hs}}-1]ds\}\sin\theta_i,$$

$$K_{ij}^{12}=-\frac{e_{15}}{2\pi}\{\frac{(x_i-x_j)}{(y_i-y_j)^2+(x_i-x_j)^2}$$

$$+\int_0^\infty \sin[s(x_i-x_j)]e^{s(y_i-y_j)}[\frac{(1-e^{-2s(h+y_i)})(1-e^{2sy_j})}{1-e^{-2hs}}-1]ds\}\cos\theta_i$$

$$+\frac{e_{15}}{2\pi}\{-\frac{y_i-y_j}{(y_i-y_j)^2+(x_i-x_j)^2}$$

$$+\int_0^\infty \cos[s(x_i-x_j)]e^{s(y_i-y_j)}[\frac{(1+e^{-2s(h+y_i)})(1-e^{2sy_j})}{1-e^{-2hs}}-1]ds\}\sin\theta_i,$$

$$K_{ij}^{21} = -\frac{e_{15}}{2\pi}\{\frac{x_i - x_j}{(x - x_j)^2 + (y_i - y_j)^2}$$

$$+\int_0^\infty \sin[s(x_i - x_j)]\mathrm{e}^{s(y_i - y_j)}[\frac{(1-\mathrm{e}^{-2s(h+y_i)})(1-\mathrm{e}^{2sy_j})}{1-e^{-2hs}} - 1]ds\}\cos\theta_i$$

$$+\frac{e_{15}}{2\pi}\{-\frac{y_i - y_j}{(x_i - x_j)^2 + (y_i - y_j)^2}$$

$$+\int_0^\infty \cos[s(x_i - x_j)]\mathrm{e}^{s(y_i - y_j)}[\frac{(1+e^{-2s(h+y_i)})(1-\mathrm{e}^{2sy_j})}{1-e^{-2hs}} - 1]ds\}\sin\theta_i ,$$

$$K_{ij}^{22} = \frac{d_{11}}{2\pi}\{\frac{x_i - x_j}{(x_i - x_j)^2 + (y_i - y_j)^2}$$

$$+\int_0^\infty \sin[s(x_i - x_j)]\mathrm{e}^{s(y_i - y_j)}[\frac{(1-\mathrm{e}^{-2s(h+y_i)})(1-\mathrm{e}^{2sy_j})}{1-e^{-2hs}} - 1]ds\}\cos\theta_i$$

$$-\frac{d_{11}}{2\pi}\{-\frac{y_i - y_j}{(x_i - x_j)^2 + (y_i - y_j)^2}$$

$$+\int_0^\infty \cos[s(x_i - x_j)]\mathrm{e}^{s(y_i - y_j)}[\frac{(1+e^{-2s(h+y_i)})(1-\mathrm{e}^{2sy_j})}{1-e^{-2hs}} - 1]ds\}\sin\theta_i , \quad -h < y_i < y_j .$$

چکیده

در این مطالعه رفتار ترک واقع در لایه پیزوالکتریک متصل به دو نیم صفحه ارتوتروپیک، با در نظر گرفتن شرایط نفوذپذیری و نفوذناپذیری سطح ترک بدست آمد. در ابتدا حل تحلیلی نابجایی الکتروالاستیک در لایه پیزوالکتریک با استفاده از تبدیل فوریه بدست آمده است. سپس به کمک روش توزیع نابجایی مجموعه معادلات انتگرالی با تکینگی های کوشی برای محیط حاوی چندین ترک تحت بار الکترومکانیکی بدست آمده است. با حل عددی معادلات انتگرالی و محاسبه دانسیته های نابجایی بر روی سطوح ترک ها، از آن برای محاسبه ضرایب شدت تنش مکانیکی و جابجایی الکتریکی استفاده شده است.

نتایج عددی نشان داد که ضرایب شدت تنش و جابجایی الکتریکی به هندسه ترکها، اندازه بار مکانیکی، اندازه و جهت بار الکتریکی بستگی دارد.